Drying Technology

An International Journal

ISSN: 0737-3937 (Print) 1532-2300 (Online) Journal homepage: http://www.tandfonline.com/loi/ldrt20

Numerical Evaluation of Optimal Approaches for Electro-Osmosis Dewatering

Jiao Yuan & Michael A. Hicks

To cite this article: Jiao Yuan & Michael A. Hicks (2017): Numerical Evaluation of Optimal Approaches for Electro-Osmosis Dewatering, Drying Technology, DOI: 10.1080/07373937.2017.1367693

To link to this article: http://dx.doi.org/10.1080/07373937.2017.1367693

Accepted author version posted online: 21 Aug 2017.

Numerical evaluation of optimal approaches for electro-osmosis dewatering

Jiao Yuan

State Key Laboratory of Geomechanics and Geotechnical Engineering, Institute of Rock and Soil Mechanics, Chinese Academy of Sciences, Wuhan, Hubei, China

Section of Geo-Engineering, Department of Geoscience and Engineering, Faculty of Civil Engineering and Geosciences, Delft University of Technology, Delft, The Netherlands

School of Civil Engineering, Sun Yat-Sen University, Xingang Xi Road, Guangzhou, China

Michael A. Hicks

Section of Geo-Engineering, Department of Geoscience and Engineering, Faculty of Civil Engineering and Geosciences, Delft University of Technology, Delft, The Netherlands

Address correspondence to Jiao Yuan. E-mail: yuanxingyu01@126.com

ABSTRACT

A newly developed numerical model is used to identify and evaluate optimum electrode configurations for electro-osmosis dewatering, as well as to evaluate approaches such as current intermittence and current reversal. Various electrode configurations, electrode spacings and voltage gradients are studied numerically using 3D models with a cubic domain and vertically installed tube electrodes. The results indicate that, with more anodes installed, one can expect more water to drain out and a more uniform surface settlement, although a greater energy consumption

is then required. A 2D square domain is used to study current intermittence and current reversal. Current intermittence allows more water to be drained out and has a higher energy efficiency compared to a continuous current, although it consumes more energy. Polarity reversal is also shown to be more efficient than a continuous current supply.

KEYWORDS: current intermittence and reversal, electrode configuration, electro-osmosis dewatering, energy consumption, numerical modelling

1. Introduction

The dewatering of soft clay creates a lot of problems in foundation engineering. In particular, because of the very low permeability of clay, primary consolidation takes a long time to complete. To shorten this dewatering time, traditional dewatering techniques such as surcharge or preloading, a combination of preloading with prefabricated vertical drains (PVD), and vacuum preloading have been used for many decades [4],[10],[17],[35],[55]. However, when dealing with materials with low rates of consolidation, low bearing capacity or shear strength, or high compressibility, such as with mine tailings [6],[14], dredged coastal sediments [37],[39],[41],[49] and municipal sludge [18],[31],[43],[46],[48], new technologies such as electro-osmosis consolidation are often needed. Electro-osmosis is a process that induces the flow of pore fluid in a soil mass from the anode to the cathode, in response to the application of a direct current electric field. The electrodes are generally installed in pairs in the soil mass, between which the direct current forces ions in the mobile part of the electric double layer (EDL) to move to the cathode, dragging water flow with them. Because of this, electro-osmosis permeability is independent of grain size, in contrast to hydraulic permeability which is dependent on grain size. As the flow caused by an electric field is often much greater than that caused by a hydraulic gradient, this means that electro-

osmosis has an advantage over conventional treatment, because it accelerates the consolidation process.

The application of electro-osmosis consolidation has been reported since the 1930s for the strengthening of soft clay in slope stabilization work. Since then, various successful field applications have been reported, such as in combatting excavation-induced heave in Norwegian quick clay [5], the strengthening of a dry dock embankment in Singapore [8], the strengthening of a soft sensitive clayey highway embankment in Canada [7], the dewatering of land reclaimed from the sea in Singapore [9] and the strengthening of slopes and embankments [22],[29]. At the same time, numerous laboratory studies have been conducted, to gain insight and to improve the performance of electro-osmosis consolidation. In particular, the influence of the electrode materials and the voltage loss at the soil−electrode interfaces has been studied [27],[47], with some results indicating that the voltage drop is less in metallic anodes than in anodes made of other materials [27]. Wu et al. [45] conducted a series of laboratory tests and founded that copper exhibited the best performance for electro-osmosis in bentonite. However, it is well known that metallic electrodes have corrosion problems which reduces their efficiency over time. Hence many attempts have been made to develop new electrode materials, with newly developed products such as electric-kinetic geosynthetics (EKG) [14],[15],[19],[21],[22] and polymeric electrical vertical drains (EVD) [9],[20],[37],[38] having been recently used as electrodes for electro-osmosis consolidation. On the other hand, chemical treatments have been introduced to improve soil−electrode contacts, as chemical injection at the electrodes has been demonstrated to enhance the transfer of electric potential to the soil [3],[7],[11],[23],[32],[33].

The area of influence of an electric field for electro-osmosis remediation, for different electrode configurations, was studied numerically by [2], with their analysis identifying the

relationship between the minimum cost and electrode spacing. A field trial on sludge using electro-osmosis was reported by Glendinning et al. [15], in which the treatment time and power consumption of two electrode configurations were studied. Recently, Hu and Wu [16] studied the settlement arising from three electrode configurations using a finite element model, whereas Tao et al. [42] studied the optimal electrode configuration for electro-osmosis dewatering by laboratory experiments and theoretical analyses. Ou et al. [33] conducted a series of electro-osmosis tests with chemical injection using different electrode sizes, voltages and electrode spacings.

The continuous application of electric current can induce excessive electrode corrosion and high heat generation, which results in an ineffective use of electro-osmosis consolidation. Lockhart and Hart [24] found that the use of current intermittence in laboratory tests improved the efficiency of electro-osmosis consolidation with respect to continuous current application. Micic et al. [26] conducted an experimental investigation into the electro-osmosis strengthening of a marine sediment, with the results demonstrating that the power consumption and electrode corrosion were reduced by using current intermittence. Mohamedelhassan and Shang [27] reported that, in their experimental research, higher electro-osmosis flow was generated with current intermittence than with a continuous current. Naggar and Routledge [30] employed electro-osmosis treatment to increase the axial and lateral capacity of piles in a laboratory experimental programme, and demonstrated that the energy consumption was greater for the constant current than the intermittent current. [5] reported the application of current reversal (also known as polarity reversal) in a field test. Wan and Mitchell [44] found that current reversal can produce a more uniform water content decrease, and thereby strength increase, between electrodes. Shang [34] found that current reversal can balance the pH of water at the electrodes, thereby reducing electrode corrosion. Recently, Yu et al. [49] conducted an experimental study on electro-osmosis combined with stack preloading to

improve the characteristics of a marine-dredged fill, using both intermittent current and polarity reversal.

The aim of this paper is to numerically investigate various factors for achieving an optimal dewatering effect during electro-osmosis. The first objective is to determine the best electrode configuration for effective dewatering, including the consideration of different electrode spacings and applied voltage levels. Further objectives are to demonstrate the efficiency of current intermittence and current reversal, compared to continuous current, during electro-osmosis consolidation. The paper starts by summarizing the numerical model used in the simulations, and then the details of the numerical analyses are presented. The settlement, pore water pressure, degree of saturation, outflow rate of water, accumulated volume of water, and electric current, as well as the power consumption of different setups, are illustrated through these examples. The criterion of energy consumption per unit volume of water discharged (also referred to as the energy index) is employed to evaluate the efficiency of the electro-osmosis consolidation. Moreover, the coefficient of variation of surface settlement is introduced, to evaluate the uniformity of consolidation between the electrodes due to electro-osmosis treatment. Hence the numerical simulations provide a strategy for assessing future field applications. The numerical tool has potential for comparing the cost of electro-osmosis consolidation with other conventional consolidation methods, by calculating the energy consumption.

2. Methodology

2.1. Modelling framework

A finite strain numerical model [50],[51],[52],[53],[54], which considers coupled electro-osmosis flow under hydraulic and electric potential gradients in a deformable porous medium under

isothermal conditions, is used to conduct the numerical experiments in this paper. The model incorporates elasto-plasticity to describe soil mechanical behaviour under unsaturated conditions, using the Barcelona Basic Model (BBM) [1]. Void ratio dependent and degree of saturation dependent empirical expressions are employed to consider the nonlinear variation of the transport parameters. The governing equations of the finite strain numerical model are provided in Yuan et al. [51] and Yuan and Hicks [50],[52],[54], and are therefore only summarized here.

Following large strain porous media theory, the kinematics and deformations of the solid skeleton are described with respect to Lagrangian coordinates, whereas those of the pore water are described using Eulerian coordinates with respect to the current configuration of the solid skeleton when the Updated Lagrangian method is employed.

The momentum balance of the soil−fluid mixture states that

$$\nabla \cdot \boldsymbol{\sigma} + \mathbf{b} = \mathbf{0} \quad (1)$$

where σ is the Cauchy total stress vector and **b** is the body force vector. According to the principle of effective stress, the total stress is equal to the sum of the effective stress, $\boldsymbol{\sigma}'$, and the pore water pressure, p, i.e.

$$\boldsymbol{\sigma} = \boldsymbol{\sigma}' + S_{\mathrm{w}} p \mathbf{I} \quad (2)$$

where S_{w} is the degree of water saturation and **I** is a unit vector.

Considering the soil particles to be incompressible, the mass conservation of the pore water can be expressed by

$$\left(\frac{nS_{\mathrm{w}}}{K_{\mathrm{w}}} - n\frac{\partial S_{\mathrm{w}}}{\partial s}\right)\frac{\partial p}{\partial t} + S_{\mathrm{w}} \nabla \cdot \mathbf{v}^{\mathrm{s}} + \nabla \cdot \bar{\mathbf{v}} = 0 \quad (3)$$

where n is the porosity of the soil, K_w is the bulk modulus of water, s is the suction, $\mathbf{v}^s$ is the velocity of the solid skeleton, $\bar{\mathbf{v}}$ is the filtration velocity of the pore water, and t is the time. According to Esrig's [13] assumption, the velocity of the pore water in the soil comprises two components. One is the hydraulic flow caused by the gradient of the pore water pressure and the other is the electro-osmosis flow caused by the electrical potential gradient. Hence,

$$\bar{\mathbf{v}} = nS_w\mathbf{v}^{ws} = -\frac{\mathbf{k}_w k_{rw}}{\gamma_w}(\nabla p - \rho^w \mathbf{g}) - \mathbf{k}_{eo}k_{reo}\nabla V \tag{4}$$

where $\mathbf{v}^{ws} = \mathbf{v}^w - \mathbf{v}^s$ is the velocity of the pore water relative to the solid skeleton, and k_{rw}, $\langle\iota\tau\lambda\rangle\gamma\langle/\iota\tau\lambda\rangle_w$, $\langle\iota\tau\lambda\rangle\rho\langle/\iota\tau\lambda\rangle^w$ and $\mathbf{g}$ are the coefficient of relative hydraulic conductivity, the unit weight of water, the density of water and the gravity acceleration, respectively. k_{reo} is the coefficient of relative electro-osmosis conductivity and V is the electrical potential. $\mathbf{k}_w$ and $\mathbf{k}_{eo}$ are the intrinsic hydraulic conductivity and electro-osmosis permeability matrices, respectively.

According to Ohm's law, the electric current density can be expressed by

$$\mathbf{j} = -k_{r\sigma e}\mathbf{k}_{\sigma e}\nabla V \tag{5}$$

where $k_{r\sigma e}$ is the relative electrical conductivity of the soil and $\mathbf{k}_{\sigma e}$ is the intrinsic electrical conductivity matrix. By applying the conservation of charge, the governing equation for the electric field can be represented by

$$-\nabla\cdot\mathbf{j} = C_p\frac{\partial V}{\partial t} \tag{6}$$

where C_p is the electrical capacitance per unit volume. As the electrical capacitance of the soil can be considered negligible, $C_p = 0$ is assumed in this paper.

2.2. Power consumption and energy index

The efficiency of electro-osmosis consolidation can be evaluated by several performance metrics, such as the power consumption, the settlement achieved or volume of water drained out, or the time elapsed to achieve a certain settlement. The two key outputs of the consolidation process are the power consumption and water drained out, as they determine the feasibility of the application. The optimal application is to discharge a sufficiently high volume of water out of the soil, given a relatively small energy consumption and short elapsed time. Hence, a more meaningful criterion, the energy index (kWh/m^3), is introduced here to evaluate the economic efficiency of electro-osmosis consolidation. This is defined as the power consumption to drain one cubic meter of water out of the soil mass, and is a function of the voltage and current, i.e.

$$E = \frac{W}{vol} = \frac{1}{vol}\int VIdt \quad (7)$$

where W is the power consumption, in kWh, vol is the accumulated volume of water discharged from the soil, in m^3, and I is the current, in, A.. In addition, in order to take account of the factors that are important in electro-osmosis dewatering, such as the processing time, the power consumption and the total mass of the treated dry solids, a simplified quantitative operating criterion, KSI, recently introduced by Mahmoud et al. [25] has also been employed here to quantify the optimal economic efficiency of the electro-osmosis dewatering. The KSI criterion is defined as

$$KSI = \left(W/m_{DS}\right)\cdot\left(t/m_{DS}\right) \quad (8)$$

where m_{DS} is the total mass of the treated dry solids, in kg.

3. Numerical Examples

This section reviews the three numerical simulations, which are conducted under large strain conditions and consider unsaturated soil behaviour by employing the BBM constitutive model. The basic material parameters for the BBM model are listed in **Table 1**, and are derived from Mohamedelhassan and Shang's [28] laboratory tests on the electro-osmosis of a marine sediment. Additional material parameters, that are needed for the BBM with Bishop's effective stress, are adopted from Sheng et al. [36] and listed in **Table 2**. Moreover, to model the dependence of relevant parameters on the degree of saturation, the following empirical expressions have been adopted [40]:

$$\begin{aligned} S_{\mathrm{w}} &= (1+(\alpha s)^{n_1})^{-m_1} \\ k_{\mathrm{rw}} &= a_{\mathrm{w}}(S_{\mathrm{w}})^{b_{\mathrm{w}}} \\ k_{\mathrm{reo}} &= a_{\mathrm{eo}}(S_{\mathrm{w}})^{b_{\mathrm{eo}}} \\ k_{\mathrm{r\sigma e}} &= a_{\mathrm{e}}(S_{\mathrm{w}})^{b_{\mathrm{e}}} \end{aligned} \qquad (9)$$

where n_1 = 1.31, m_1 = 1–1/n_1, <ιτλ>α </ιτλ> = 0.00851kPa $^{-1}$, a_{w} = 1, b_{w} = 5, a_{eo} = 1, b_{eo} = 3.2, a_{e} = 1 and b_{e} = 2.

The transport parameters are also selected from the tests of Mohamedelhassan and Shang [28], in the form of the following empirical expressions:

$$\begin{aligned} \log k_{\mathrm{w}} &= 1.1075e - 11.297 \\ k_{\mathrm{eo}} &= 3.27\times10^{-8}n - 1.14\times10^{-8} \\ k_{\sigma\mathrm{e}} &= \frac{0.42(1+e)}{1.29+0.33e} \end{aligned} \qquad (10)$$

where e is the void ratio of the soil.

In all examples, the initial effective stresses have been assigned by using the effective unit weight of the soil and the coefficient of earth pressure at rest. The initial yield surface location is determined according to the effective pressure and assumed over-consolidation ratio. The initial pore water pressures are assumed to be hydrostatic and the soil is considered to be initially fully saturated. Note that the current model formulation does not set a limit on the tensile pore pressures generated, for example, to account for the effects of cavitation. The model domains, boundary conditions and other details are described as follows.

3.1. Example 1: Electrode configurations

3D models are used to investigate the efficiency of various electrode configurations, electrode spacings and voltage gradients. The main focus is to find the optimum electrode configuration; that is, the one with the lowest energy index. The domain is a $1m^3$ cube and the electrodes are assumed to be 0.02m in diameter and 0.75m long. In general, electrode configurations are designed to generate axi-symmetric (or radial) flow and produce straight-line flow paths to the cathode [2],[15]. So, this example focuses on a single centrally located cathode, out through which water flows, surrounded by anodes that are installed at a specific distance from the cathode to achieve radial flow. The effect of the number of anodes surrounding the cathode, as well as the distance between the cathode and each anode, and different applied voltage gradients, is studied.

Three electrode configurations that have been used in practical applications [5],[7],[14],[15] are simulated here, initially with an electrode spacing of 0.3m and a voltage of 5V applied at the anodes. **Figure 1** shows a plan view of the three configurations. In configuration, A.; one cathode and two anodes are installed in a single row located in the middle of the domain. In configuration,

B.; one central cathode is surrounded by four anodes. In configuration, C.; a central cathode is surrounded by six anodes in a hexagonal pattern. In the second part of the numerical example, the effect of electrode spacing and voltage gradient are studied using electrode configuration, B.. The performance of electrode spacings of 0.2, 0.3 and 0.4m is investigated. In the scenario with the different voltage gradients, applied voltages of 5, 7.5 and 10V are investigated.

Although 3D analyses are carried out to simulate the conditions imposed on the cubic domain, only 1/4, 1/8 and 1/4 of the domain are considered, due to the planes of symmetry for configurations, A.; B and, C.; respectively. **Figure 2** shows the geometries and meshes used in the analyses (generated by the commercial software package COMSOL Multiphysics 5.1 [12]. The mesh boundary conditions are that the vertical sides are prevented from moving in the horizontal plane, whereas the bottom boundary is fixed. In terms of hydraulic boundary conditions, the top surface is open and free draining, whereas the remaining boundaries are impermeable; in order to maintain a draining condition at the cathode, a hydraulic conductivity of 1.0×10^{-4}m /s is assumed for the cathode elements. For the electrical boundary conditions, the relevant voltages are maintained at the top of the anode and cathode, whereas all other boundaries are assumed to be impermeable to electric current. Note that, to represent steel electrodes, an electrical conductivity of 1.0×10^{6}S /m is assumed, whereas the transport parameters of the soil elements are assigned by using the initial void ratio (which is related to the initial stresses) and Eq. (10). A four-node tetrahedron finite element is adopted for the displacements, pore water pressure and electrical potential.

3.2. Example 2: Current intermittence

Current intermittence is the application of a pulse voltage at predetermined on/off intervals during the electro-osmosis consolidation. Recent experimental research has indicated that an intermittent current is beneficial to electro-osmosis consolidation compared to a continuous current [28]. A 2D square domain of 1m side length and unit thickness (see **Figure 3**) is used in the investigation. The boundary conditions are as follows: the left edge is impermeable and on rollers allowing only vertical movement; the right edge is free draining and on rollers allowing only vertical movement; the bottom boundary is impermeable and fixed; and the top boundary is free draining. In terms of electrical boundary conditions: the anode is along the left edge, the right edge is the cathode, and the horizontal boundaries are impermeable to electric current.

For both simulations (continuous and intermittent current), the power-on time is 5×10^6 seconds. For the intermittent current analyses, the total simulation time is 9×10^6 seconds and there are four intermittences in the applied input voltage, each lasting for 1×10^6 seconds, as shown in **Figure 4a**. In this example, an eight-node quadrilateral finite element is adopted for displacements, and this is coupled to a four node quadrilateral element for modelling pore water pressure and electrical potential.

3.3. Example 3: Current reversal

In order to study the effects of current reversal during electro-osmosis consolidation, the 2D model in **Figure 3** is subjected to a voltage of 5V , with a voltage reversal mid-way through the simulation (**Figure 4b**). The boundary conditions are the same as for Example 2 for the first 2.5×10^6 seconds, before the polarity reversal. The current is reversed at 2.5×10^6 seconds and, at this time, the hydraulic boundary conditions are also reversed: that is, the left edge (former anode)

is now free draining and the right edge (former cathode) is now impermeable. The remaining boundary conditions are the same as before the polarity reversal.

4. Results and Discussion

4.1. Electrode configurations

4.1.1 Electrode patterns

The water outflow rates through the cathode, for the three electrode configurations, are shown in **Figure 5a**. They decrease with time, due to the negative pore water pressure developed near the anode causing a hydraulic flow which is opposite to the direction of electro-osmosis flow. Hence, when the hydraulic flow equals the electro-osmosis flow the system reaches the steady state. The figure shows that, with more anodes installed around the cathode, a higher water outflow rate is achieved. **Figure 5b** shows the accumulated volume of water exiting through the cathode; as expected, with more anodes there is a greater outflow of water. Configuration B gives an outflow that is about 30% greater than that of configuration, A.; whereas configuration C indicates a rather modest additional outflow.

Figure 5c shows the evolution of electric current through the cathode. Note that, since the electrical conductivity is decreasing with both degree of water saturation and void ratio, as described by Eqs. (9) and (10), the electric current is also decreasing with time. Configuration B gives an electric current that is about 20% greater than that of configuration, A.; whereas the electric current for configuration C is only slightly greater than that of configuration, B.. The time evolution of the energy consumption, for the various electrode configurations, is shown in **Figure 5d**. The investigated electrode configurations show that, with more anodes installed, more water

is draining out and the time required to reach a certain accumulated volume of water is less, although the increase in the number of anodes results in a greater energy consumption. So, the energy index introduced in Section 2.2 is used as a criterion to evaluate and compare the consolidation effects of the various configurations. As shown in **Figure 6a**, configuration A has the lowest energy index, although the differences between the three cases are small. In order to achieve the optimum efficiency for the electro-osmosis dewatering, the value of, K. S. I.; calculated from Eq. (8), should be minimized. **Figure 6b** illustrates the KSI values for the different electrode configurations and, as for the energy index, configuration A has the lowest KSI value, indicating that configuration A gives the most energy efficient solution. The coefficients of variation of surface settlement for the three electrode configurations are shown in **Figure 6c**, in which the coefficient of variation is equal to the standard deviation of the surface settlement divided by the mean of the surface settlement. It is used here to measure the uniformity of the surface settlement; the smaller this value is, the more uniform is the settlement. It is seen that configurations B and C have much smaller coefficients of variation than configuration, A.; indicating that the surface settlement between the electrodes is more uniform for these cases.

In conclusion, configurations B and C give a larger volume of drained water and a much more uniform surface settlement profile than configuration, A.; but they also have slightly greater energy indices. Configuration A is the most efficient electrode installation, from the economic point of view, but results in the largest differential settlement. Configuration B has a slightly smaller energy index than configuration, C.; but requires only two thirds as many installed anodes to achieve almost the same volume of water drained out and gives a similar (low) coefficient of variation of the surface settlement. This suggests that, if reducing the volume of water in the soil mass and having more uniform consolidation between the electrodes are the primary objectives of

the electro-osmosis consolidation, this is best achieved by an increased number of anodes (configuration C), although it will come at the cost of increased energy consumption. If a low cost of consolidation is the objective, but with a reasonably uniform consolidation between the electrodes, then electrode configuration B is recommended.

4.1.2 Electrode spacing

Decreasing the spacing between the anodes and cathode results in a greater initial water outflow rate through the cathode, as seen in **Figure 7a**. However, this difference decreases with time, and the three spacings considered give very similar results during the latter stages of the simulations. The accumulated volume of water exiting through the cathode with time is shown in **Figure 7b**. The 0.3 and 0.4m spacing scenarios have similar final accumulated volumes of water, whereas the 0.2m spacing has a slightly higher accumulated volume of water. **Figure 7c** shows the decrease of the electric current through the cathode with time, and demonstrates that a decrease in spacing results in a greater electric current. The time evolution of the energy consumption (**Figure 7d**) shows a similar trend, with a small spacing between the electrodes resulting in greater energy consumption. Moreover, **Figure 8a** shows that a smaller electrode spacing results in a greater energy index, due to the smaller area of effective electric field; that is, a larger area of influence, as given by a larger electrode spacing, means a higher efficiency [2]. This conclusion is reinforced by the KSI criterion for the overall performance, shown in **Figure 8b**, which confirms that the lowest value is obtained for the largest electrode spacing. Overall, it is seen that, by using a greater electrode spacing, the electro-osmosis consolidation is more energy efficient, although the rate of dewatering is slightly lower than at a smaller electrode spacing.

4.1.3 Applied voltage

Many researchers have investigated experimentally the influence of voltage gradient/applied voltage for achieving the optimal rate of electro-osmosis consolidation [26],[27],[40]. [5] reported that a high voltage gradient tends to dry out the soil around the anode very rapidly, so that the true potential benefit of electro-osmosis consolidation is much reduced. In general, electro-osmosis dewatering is more energy efficient at lower voltage gradients. However, a lower voltage gradient has the obvious disadvantage that the rate of consolidation is lower than at higher voltage gradients, even though the energy efficiency is better.

Figure 9a shows that increasing the applied voltage (or voltage gradient) results in a greater initial water outflow rate, although the differences between the three cases become much smaller with time, and, by the ends of the analyses, the highest voltage case is seen to have the lowest water outflow rate. However, the larger voltage gradient results in a greater volume of water collected from the cathode over the duration of the analysis (**Figure 9b**). There is clearly a nonlinear relationship between the volume of water collected from the cathode and the voltage gradient, which is likely to be due to the transport parameters decreasing with void ratio and degree of water saturation, which causes a reduction in the efficiency of the system. Moreover, **Figure 9c** shows that, whereas the electric current is proportional to the voltage at the start of the analyses, the relationship becomes nonlinear as the electric current reduces over time. For the scenarios with high voltage levels (7.5 and 10V), the electric current decreases more rapidly with time than for the low voltage level case (5V). The time evolution of the energy consumption for the three voltage gradients is shown in **Figure 9d**. As expected, increasing the applied voltage at the anodes results in greater energy consumption. **Figure 10** shows that it also results in a significantly greater energy index and KSI criterion, indicating lower energy efficiency.

4.2. Current intermittence

Figure 11a shows the evolution of pore water pressure with time at the bottom of the anode for continuous and intermittent applied currents. In order to better compare the results, the current-off times are not included in this and following figures; therefore, both simulations have the same *x* axis length. As can be seen, the pore water pressure drops significantly during each period of current-off, due to the pore water pressure redistributing within the domain. The final pore water pressure developed in the current intermittent case is much smaller than in the continuous case. Moreover, as a result of the pore water pressure drops, the settlement at the top of the anode rebounds slightly during each period of current-off time (**Figure 11b**), and the current intermittent case gives a lower final absolute settlement compared to the continuous case. **Figure 11c** shows the water outflow rate through the cathode for continuous and intermittent applied currents. There is a gradual reduction in the overall flow rate as the consolidation progresses, with a peak in the flow rate observed when the current is reapplied after each period of zero current (i.e. in the intermittent case). This is because of the partial dissipation of negative pore water pressure during the current-off period, due to the redistribution of pore water within the domain; according to Eq. (4), if the voltage potential is constant the outflow rate will increase if the negative pore water pressure decreases, and so, after a current intermittence, the outflow rate is much bigger than in the continuous current approach. Note that the small drop in outflow rate at the beginning of the simulation is due to the hydraulic conductivity being very small. Hence, the bulk of the water cannot flow out immediately, but remains in the middle of the domain causing a positive pore water pressure; this makes the water outflow rate drop temporarily, but, as the positive pore water pressures dissipate, the water outflow rate recovers. The evolution of accumulated volume of water exiting through the cathode, for intermittent and continuous currents, is shown in **Figure 11d**. It is seen that, before 2×10^6 seconds, the accumulated volume of water for both simulations is almost

the same. However, as the consolidation progresses, the volume of water accumulated from the intermittent current is greater than that from the continuous current, due to the increase in the outflow rate each time the current is reapplied.

The evolution of electric current through the cathode has a similar trend to the water outflow rate. As shown in **Figure 11e**, a brief peak in the current is found when the voltage is reapplied; indeed, this is a common observation during laboratory tests of electro-osmosis [13]. As explained before, the negative pore water pressures developed near the anode will dissipate as the water redistributes within the domain, and the soil deformation will rebound slightly when the current is off. Due to the degree of water saturation and soil void ratio both increasing, according to Eqs. (9) and (10), the electric conductivity will therefore increase when the current is off. Hence, when the voltage is reapplied after a period of zero voltage, the electric current will peak. As a higher current is obtained after the current is intermitted, a slightly higher energy consumption compared to a continuous current is apparent, as seen in **Figure 11f**. However, the volume of water drained out of the soil is also greater compared to the continuous current. Hence in order to evaluate the efficiency of both methods, the energy index is plotted in **Figure 12a**. It is seen that the energy index for the intermittent current is around 17% smaller than that for the continuous current, which indicates that current intermittence can reduce the power consumption required to drain a certain volume of water, thereby enhancing the effectiveness of electro-osmosis treatment. In contrast, the KSI criterion (**Figure 12b**) for the intermittent current is approximately double that for the continuous current. This is because, although current intermittence is more energy efficient, it takes almost twice as much treatment time compared to the continuous case. When taking account of the treatment time, the continuous current scenario achieves the best strategy time/energy compromise.

In order to further highlight the differences between continuous and intermittent current analyses, the contours of pore water pressure at different times are presented in **Figure 13**. Firstly, **Figure 13a-d** shows how the pore water pressure has redistributed within the domain by the end of each of the first four current-off periods. When the accumulated current-on time has been relatively short (**Figure 13a-b**), a negative pore water pressure can only be observed at the bottom of the anode and/or the top of the domain. On the other hand, after a relatively long accumulated current-on time (**Figure 13c-d**), the negative pore water pressure can be observed over most of the domain except around the bottom of the cathode. **Figure 13e-f** compares the final pore water pressure spatial distributions for the continuous and intermittent cases; although similar pore water pressure profiles are observed, larger maximum negative pore water pressures are found in the continuous analysis.

4.3. Current reversal

The impact of reversing the electric current (at 2.5×10^6s) is compared to the case of no current reversal in **Figures 14** and **15**. The results suggest that soil samples tested using current reversal have a higher cathode surface settlement than those conducted using a continuous current. With current reversal, there is only a slight settlement rebound found at the top of the original anode, but a much higher surface settlement is obtained at the top of the original cathode (even higher than the settlement at the anode without current reversal), as shown in **Figure 14a**.

The effect of current reversal is that the water outflow rate is decreased to almost zero immediately after the reversal and then it increases rapidly to a value which is greater than that for the continuous current (**Figure 14b**), resulting in a greater volume of water accumulated through the cathode after 3×10^6 seconds compared to when a continuous current is applied (**Figure 14c**).

This is because, after current reversal, the negative pore water pressures near the former anode are not dissipated immediately, which causes a local hydraulic flow that is in the opposite direction to the electro-osmosis flow; hence the water outflow rate decreases to zero at the new cathode. However, when the current is reversed the hydraulic boundary conditions are also reversed and so the left edge becomes open for free drainage; hence the negative pore water pressure can dissipate rapidly, while, at the same time, the outflow rate increases rapidly. Because of the water redistribution within the domain after the current is reversed, the soil becomes more saturated, resulting in an enhanced water outflow rate compared to the case with no current reversal, as seen in **Figure 14b**.

Figure 14d shows the electric current through the cathode versus time, for both the continuous and current reversal cases, showing that the current decreases gradually as the consolidation progresses. However, there is a slight increase in the current to a peak value immediately after the current is reversed, followed by a reduction of the current at a rate that is greater than that for a continuous current. The evolution of energy consumption is shown in **Figure 14e**. It is seen that current reversal results in no noticeable increase in energy consumption, due to the current decreasing more rapidly after the initial peak current, as seen in **Figure 14d**. However, the simulation with current reversal requires less energy consumption per volume of water drained out of the soil, as seen in **Figure 15a**, despite the energy consumption being almost the same, due to the greater volume of water being drained compared to the continuous current case. Hence the energy index is around 15% smaller for current reversal. Moreover, due to the power consumptions for both cases being almost identical during the same treatment period, they achieve almost the same KSI values, as seen in **Figure 15b**.

5. Conclusions

Various electrode configurations, as well as current intermittence and current reversal approaches for electro-osmosis consolidation have been investigated using numerical simulation. 3D and 2D domains have been analyzed to simulate the time dependent behaviour of the settlement, pore water pressure, outflow rate of water, accumulated volume of water and electric current, as well as the energy consumption of different setups. In particular, the combination of a nonlinear elasto-plastic constitutive model and relationships for hydraulic conductivity, electro-osmosis permeability and electrical conductivity as a function of the void ratio and degree of water saturation, have allowed the model to capture the coupled nonlinear response during electro-osmosis consolidation at large strain.

Three electrode configurations have been analyzed using a 3D model domain, with the simulation results indicating that a greater number of anodes installed around the central cathode leads to expedited consolidation and an increased settlement, albeit with greater energy consumption. Increasing the electrode spacing resulted in an increase in the extent the effective electric field and thus an increase in the energy efficiency of the electro-osmosis consolidation, although it resulted in a lower rate of dewatering. Decreasing the voltage gradient also resulted in higher energy efficiency, but with a lower rate of dewatering. The nonlinear response between the energy index and surface settlement indicates the need to optimize the approach for each particular application.

2D simulations comparing the performance of intermittent and continuous currents have shown that, in general, intermittent current leads to a greater volume of water being drained from the soil. However, it has also been shown that the energy consumption for an intermittent current is greater than that for a continuous current. By computing the energy index of both simulations,

it is concluded that the efficiency of electro-osmosis consolidation is greater when using current intermittence.

The results of a numerical simulation using current reversal have shown that the reversal of the electric field enhances consolidation between the electrodes, as indicated by a higher surface settlement at the original cathode when current reversal was used. Moreover, the results have demonstrated the greater efficiency of the consolidation with current reversal than with a continuous current.

The findings of the numerical simulations in this paper are consistent with those reported in previous laboratory and field tests, and provide further insight into the processes involved in electro-osmosis consolidation. Due to the considerations of consolidation time, energy consumption and uniformity of consolidation for a particular application, the use of numerical modelling has a potential use in optimizing the design of field applications involving electro-osmosis consolidation.

Acknowledgements

The authors are grateful to the China Scholarship Council, the Geo-Engineering Section of Delft University of Technology as well as the open research fund of State Key Laboratory of Geomechanics and Geotechnical Engineering, Institute of Rock and Soil Mechanics, Chinese Academy of Science (Grant No. Z016004) for financial support of the first author.

References

[1] Alonso, E. E.; Gens, A.; Josa, A. A Constitutive Model for Partially Saturated Soils. *Geotechnique* **1990**, *40*(3), 405–430. doi:10.1680/geot.1990.40.3.405

[2] Alshawabkeh, A. N.; Gale, R. J.; Ozsu-Acar, E.; Bricka, R. M. Optimization of 2-D Electrode Configuration for Electrokinetic Remediation. *Journal of Soil Contamination* **1999**, *8*(6), 617–635.
[3] Asavadorndeja, P.; Glawe, U. Electrokinetic Strengthening of Soft Clay using the Anode Depolarization Method. *Bulletin of Engineering Geology and the Environment* **2005**, *64*(3), 237–245. doi:10.1007/s10064-005-0276-7
[4] Bergado, D. T.; Balasubramaniam, A. S.; Fannin, R. J.; Holtz, R. D. Prefabricated Vertical Drains (PVDs) in Soft Bangkok Clay: A Case Study of the New Bangkok International Airport Project. *Canadian Geotechnical Journal* **2002**, *39*(2), 304–315. doi:10.1139/t01-100
[5] Bjerrum, L.; Moum, J.; Eide, O. Application of Electro-Osmosis to a Foundation Problem in a Norwegian Quick Clay. *Geotechnique* **1967**, *17*(3), 214–235. doi:10.1680/geot.1967.17.3.214
[6] Bourgès-Gastaud, S.; Stoltz, G.; Dolez, P.; Blond, É.; Touze-Foltz, N. Laboratory Device to Characterize Electrokinetic Geocomposites for Fluid Fine Tailings Dewatering. *Canadian Geotechnical Journal* **2014**, *52*(4), 505–514. doi:10.1139/cgj-2014-0031
[7] Burnotte, F.; Lefebvre, G.; Grondin, G. A Case Record of Electroosmotic Consolidation of Soft Clay with Improved Soil Electrode Contact. *Canadian Geotechnical Journal* **2004**, *41*(6), 1038–1053. doi:10.1139/t04-045
[8] Chappell, B. A.; Burton, P. L. Electro-Osmosis Applied to Unstable Embankment. *Journal of the Geotechnical Engineering Division, ASCE* **1975**, *101*(8), 733–740.
[9] Chew, S. H.; Karunaratne, G. P.; Kuma, V. M.; Lim, L. H.; Toh, M. L.; Hee, A. M. A Field Trial for Soft Clay Consolidation using Electric Vertical Drains. *Geotextiles and Geomembranes* **2004**, *22*(1–2), 17–35. doi:10.1016/s0266-1144(03)00049-9
[10] Chu, J.; Yan, S. W.; Yang, H. Soil Improvement by the Vacuum Preloading Method for an oil Storage Station. *Geotechnique* **2000**, *50*(6), 625–632.
[11] Citeau, M.; Loginov, M.; Vorobiev, E. Improvement of Sludge Electrodewatering by Anode Flushing. *Drying Technology* **2016**, *34*(3), 307–317. doi:10.1080/07373937.2015.1052083
[12] Comsol, A. B. COMSOL Multiphysics 5.1, 2015.
[13] Esrig, M. I. Pore Pressures, Consolidation and Electrokinetics. *Journal of the Geotechnical Engineering Division, ASCE* **1968**, *94*(4), 899–921.
[14] Fourie, A. B.; Johns, D. G.; Jones, C. J. F. P. Dewatering of Mine Tailings using Eletrokinetic Geosynthetics. *Canadian Geotechnical Journal* **2007**, *44*(2), 160–172. doi:10.1139/t06-112
[15] Glendinning, S.; Jones, C. J. F. P.; Lamont-Black, J.; Hall, J. Treatment of Lagooned Sewage Sludge in situ using Electrokinetic Geosynthetics. *Geosynthetics International* **2008**, *15*(3), 192–204. doi:10.1680/gein.2008.15.3.192
[16] Hu, L.; Wu, H. Mathematical Model of Electro-Osmotic Consolidation for Soft Ground Improvements. *Geotechnique* **2014**, *64*(2), 155–164.
[17] Indraratna, B.; Rujikiatkamjorn, C.; Ameratunga, J.; Boyle, P. Performance and Prediction of Vacuum Combined Surcharge Consolidation at Port of Brisbane. *Journal of Geotechnical and Geoenvironmental Engineering* **2011**, *137*(11), 1009–1018. doi:10.1061/(asce)gt.1943-5606.0000519
[18] Iwata, M.; Tanaka, T.; Jami, M. S. Application of Electroosmosis for Sludge Dewatering – A Review. *Drying Technology* **2013**, *31*(2), 170–184. doi:10.1080/07373937.2012.691592

[19] Jones, C. J. F. P.; Lamont-Black, J.; Glendinning, S. Electrokinetic Geosynthetics in Hydraulic Applications. *Geotextiles and Geomembranes* **2011**, *29*(4), 381–390. doi:10.1016/j.geotexmem.2010.11.011
[20] Karunaratne, G. P. Prefabricated and Electrical Vertical Drains for Consolidation of Soft Clay. *Geotextiles and Geomembranes* **2011**, *29*(4), 391–401. doi:10.1016/j.geotexmem.2010.12.005
[21] Lamont-Black, J.; Jones, C. J. F. P.; White, C. Electrokinetic Geosynthetic Dewatering of Nuclear Contaminated Waste. *Geotextiles and Geomembranes* **2015**, *43*(4), 359–362. doi:10.1016/j.geotexmem.2015.04.005
[22] Lamont-Black, J.; Jones, C. J. F. P.; Alder, D. Electrokinetic Strengthening of Slopes – Case History. *Geotextiles and Geomembranes* **2016**, *44*(3), 319–331. doi:10.1016/j.geotexmem.2016.01.001
[23] Lefebvre, G.; Burnotte, F. Improvements of Electroosmotic Consolidation of Soft Clays by Minimizing Power Loss at Electrodes. *Canadian Geotechnical Journal*. **2002**, *39*(2), 399–408. doi:10.1139/t01-102
[24] Lockhart, N. C.; Hart, G. H. Electro-Osmotic Dewatering of Fine Suspensions: The Efficacy of Current Interruptions. *Drying Technology* **1988**, *6*(3), 415–423. doi:10.1080/07373938808916391
[25] Mahmoud, A.; Hoadley, A. F.; Conrardy, J. B.; Olivier, J.; Vaxelaire, J. Influence of Process Operating Parameters on Dryness Level and Energy Saving during Wastewater Sludge Electro-Dewatering. *Water Research* **2016**, *103*, 109–123. doi:10.1016/j.watres.2016.07.016
[26] Micic, S.; Shang, J. Q.; Lo, K. Y.; Lee, Y. N.; Lee, S. W. Electrokinetic Strengthening of a Marine Sediment using Intermittent Current. *Canadian Geotechnical Journal* **2001**, *38*(2), 287–302. doi:10.1139/cgj-38-2-287
[27] Mohamedelhassan, E.; Shang, J. Q. Effects of Electrode Materials and Current Intermittence in Electro-Osmosis. *Proceedings of the Institution of Civil Engineers: Ground Improvement* **2001**, *5*(1), 3–11. doi:10.1680/grim.2001.5.1.3
[28] Mohamedelhassan, E.; Shang, J. Q. Feasibility Assessment of Electro-Osmotic Consolidation on Marine Sediment. *Proceedings of the Institution of Civil Engineers: Ground Improvement* **2002**, *6*(4), 145–152. doi:10.1680/grim.2002.6.4.145
[29] Mumtaz, M.; Girish, M. S. Electrokinetic Geosynthetic Stabilisation of Embankment Slopes. *International Journal of Engineering Research* **2014**, *3*(12), 766–768. doi:10.17950/ijer/v3s12/1213
[30] Naggar, M. H. E.; Routledge, S. A. Effect of Electro-Osmotic Treatment on Piles. *Proceedings of the Institution of Civil Engineers – Ground Improvement* **2004**, *8*(1), 17–31. doi:10.1680/grim.2004.8.1.17
[31] Olivier, J.; Mahmoud, A.; Vaxelaire, J.; Conrardy, J.-B., Citeau, M.; Vorobiev, E. Electro-Dewatering of Anaerobically Digested and Activated Sludges: An Energy Aspect Analysis. *Drying Technology* **2014**, *32*(9), 1091–1103. doi:10.1080/07373937.2014.884133
[32] Ou, C.-Y.; Chien, S.-C.; Chang, H.-H. Soil Improvement using Electroosmosis with the Injection of Chemical Solutions: Field Tests. *Canadian Geotechnical Journal* **2009**, *46*(6), 727–733. doi:10.1139/t09-012

[33] Ou, C.-Y.; Chien, S.-C.; Liu, R.-H. A Study of the Effects of Electrode Spacing on the Cementation Region for Electro-Osmotic Chemical Treatment. *Applied Clay Science* **2015**, *104*, 168–181. doi:10.1016/j.clay.2014.11.027

[34] Shang, J. Q. Electrokinetic Dewatering of Clay Slurries as Engineered Soil Covers. *Canadian Geotechnical Journal* **1997**, *34*(1), 78–86. doi:10.1139/cgj-34-1-78

[35] Shen, S.-L.; Chai, J.-C.; Hong, Z.-S.; Cai, F.-X. Analysis of Field Performance of Embankments on Soft Clay Deposit with and without PVD-Improvement. *Geotextiles and Geomembranes* **2005**, *23*(6), 463–485. doi:10.1016/j.geotexmem.2005.05.002

[36] Sheng, D.; Smith, D. W.; Sloan, S. W.; Gens, A. Finite Element Formulation and Algorithms for Unsaturated Soils. Part II: Verification and Application. *International Journal for Numerical and Analytical Methods in Geomechanics* **2003**, *27*(9), 767–790. doi:10.1002/nag.296

[37] Sun, Z.; Gao, M.; Yu, X. Vacuum Preloading Combined with Electro-Osmotic Dewatering of Dredger fill using Electric Vertical Drains. *Drying Technology* **2015**, *33*(7), 847–853. doi:10.1080/07373937.2014.992529

[38] Sun, Z.; Gao, M.; Yu, X. The Characteristics of Electric Vertical Drains in Electro-Osmotic Dewatering. *Drying Technology* **2017a**, *35*(3), 263–271. doi:10.1080/07373937.2016.1172084

[39] Sun, Z.; Gao, M.; Yu, X. Dewatering Effect of Vacuum Preloading Incorporated with Electro-Osmosis in Different Ways. *Drying Technology* **2017b**, *35*(1), 38–45. doi:10.1080/07373937.2016.1157602

[40] Tamagnini, C.; Jommi, C.; Cattaneo, F. A Model for Coupled Electro-Hydro-Mechanical Processes in Fine Grained Soils Accounting for Gas Generation and Transport. *Anais da Academia Brasileira de Ciencias* **2010**, *82*(1), 169–193. doi:10.1590/s0001-37652010000100014

[41] Tang, X.; Xue, Z.; Yang, Q.; Li, T.; VanSeveren, M. Water Content and Shear Strength Evaluation of Marine Soil after Electro-Osmosis Experiments. *Drying Technology* **2017**, 1–15. doi:10.1080/07373937.2016.1270299

[42] Tao, Y.; Zhou, J.; Gong, X.; Hu, P. Electro-Osmotic Dehydration of Hangzhou Sludge with Selected Electrode Arrangements. *Drying Technology* **2016**, *34*(1), 66–75. doi:10.1080/07373937.2015.1006369

[43] Tuan, P.-A., Mika, S.; Pirjo, I. Sewage Sludge Electro-Dewatering Treatment – A Review. *Drying Technology* **2012**, *30*(7), 691–706. doi:10.1080/07373937.2012.654874

[44] Wan, T.; Mitchell, J. K. Electroosmotic Consolidation of Soils. *Journal of the Geotechnical Engineering Division, ASCE* **1976**, *101*(5), 503–507.

[45] Wu, H.; Hu, L.; Wen, Q. Electro-Osmotic Enhancement of Bentonite with Reactive and Inert Electrodes. *Applied Clay Science* **2015**, *111*, 76–82. doi:10.1016/j.clay.2015.04.006

[46] Xu, H.; Ding, T. Influence of Vacuum Pressure, pH, and Potential Gradient on the Vacuum Electro-Osmosis Dewatering of Drinking Water Treatment Sludge. *Drying Technology* **2016**, *34*(9), 1107–1117. doi:10.1080/07373937.2015.1095203

[47] Xue, Z.; Tang, X.; Yang, Q.; Wan, Y.; Yang, G. Comparison of Electro-Osmosis Experiments on Marine Sludge with Different Electrode Materials. *Drying Technology* **2015**, *33*(8), 986–995. doi:10.1080/07373937.2015.1011274

[48] Yoshida, H.; Yoshikawa, T.; Kawasaki, M. Evaluation of Suitable Material Properties of Sludge for Electroosmotic Dewatering. *Drying Technology* **2013**, *31*(7), 775–784. doi:10.1080/07373937.2012.760581

[49] Yu, Z.; Zhang, Y.; Zhou, B.; Guo, L.; Li, Z.; Li, X. Laboratory Investigation of Electro-Osmosis Effects in Saturated Dredger Fill – A Comparison with the Stack Preloading. *Drying Technology* **2017**, *35*(6), 736–746. doi:10.1080/07373937.2016.1209773

[50] Yuan, J.; Hicks, M. A. Large Deformation Elastic Electro-Osmosis Consolidation of Clays. *Computers and Geotechnics* **2013**, *54*, 60–68.

[51] Yuan, J.; Hicks, M. A.; Dijkstra, J. Numerical Model of Elasto-Plastic Electro-Osmosis Consolidation of Clays. Proceedings of Poromechanics V - Proceedings of the 5th Biot Conference on Poromechanics, Vienna, Austria, ASCE, 2013.

[52] Yuan, J.; Hicks, M. A. Numerical Modelling of Electro-Osmosis Consolidation of Unsaturated Clay at Large Strain. Proceedings of Numerical Methods in Geotechnical Engineering - Proceedings of the 8th European Conference on Numerical Methods in Geotechnical Engineering, Delft, The Netherlands, CRC press, 2014.

[53] Yuan, J.; Hicks, M. A. Numerical Analysis of Electro-Osmosis Consolidation: A Case Study. *Géotechnique Letters* **2015**, *5*(3), 147–152.

[54] Yuan, J.; Hicks, M. A. Numerical Simulation of Elasto-Plastic Electro-Osmosis Consolidation at Large Strain. *Acta Geotechnica* **2016**, *11*(1), 127–143. doi:10.1007/s11440-015-0366-z

[55] Zhang, N.; Shen, S.; Wu, H.; Chai, J.; Yin, Z. Evaluation of Performance of Embankments with Reinforcement on PVD-Improved Marine Clay. *Geotextiles and Geomembrances* **2015**, *43*(6), 506–514.

Table 1. Basic material parameters for Barcelona Basic Model model (based on [28])

Void ratio at $p' = 1$kPa	e	3.95
Poisson's ratio	ν	0.3
Plastic compression index	λ	0.547
Unloading−reloading index	κ	0.064
Critical stress ratio	M	1.172
Over-consolidation ratio	OCR	1.0
Coefficient of earth pressure at rest	K_0	1.0
Total unit weight of soil	γ	19 kN/m^3

Table 2. Additional material parameters for Barcelona Basic Model (after Sheng et al. [36])

Reference stress	p_r	1.0kPa
Rate of increase of soil stiffness with suction	β	0.012kPa^{-1}
Parameter defining the maximum soil stiffness	r	0.75
Rate of cohesion increase with suction	k_s	0
Elastic compression index with respect to suction	κ_s	0
Degree of non-associativity of the flow rule	α	0.437

Figure 1. Plan view of analysed electrode configurations.

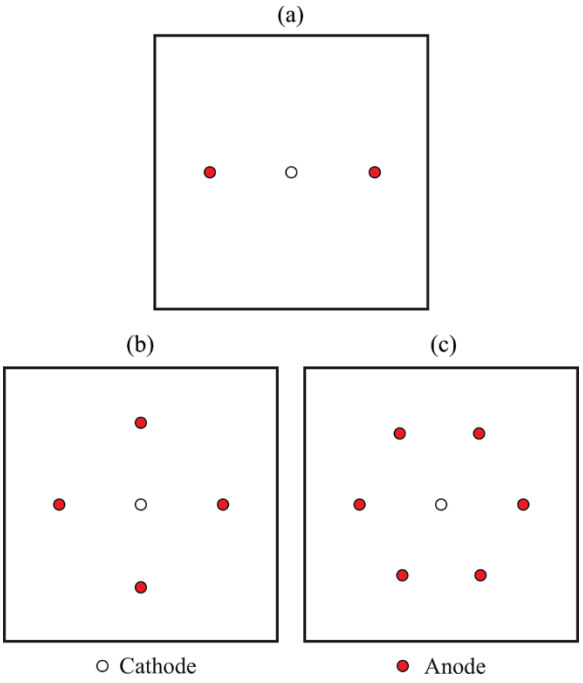

Figure 2. 3D finite element meshes for analysed electrode configurations.

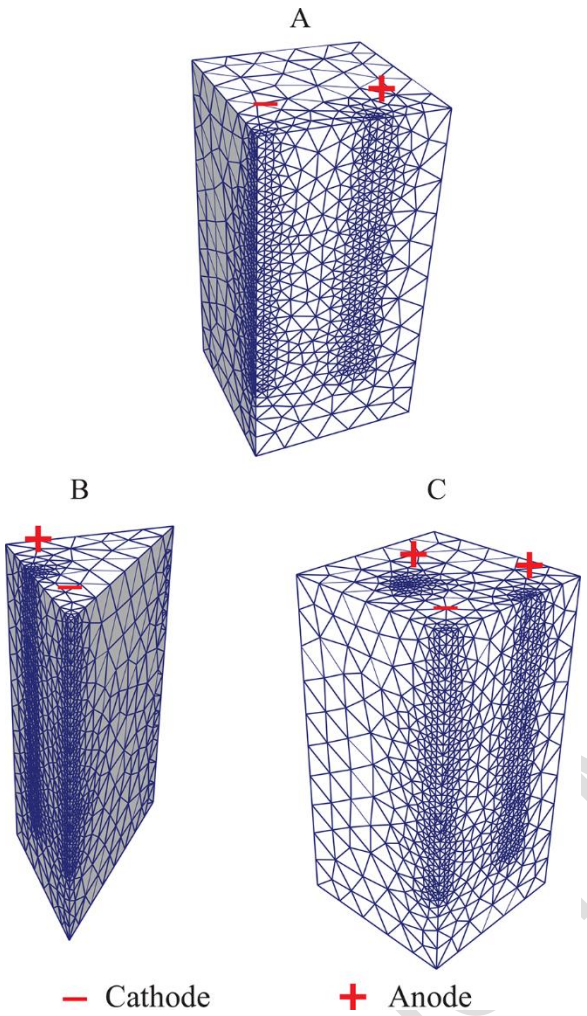

Figure 3. Model domain for simulation of current intermittence and current reversal.

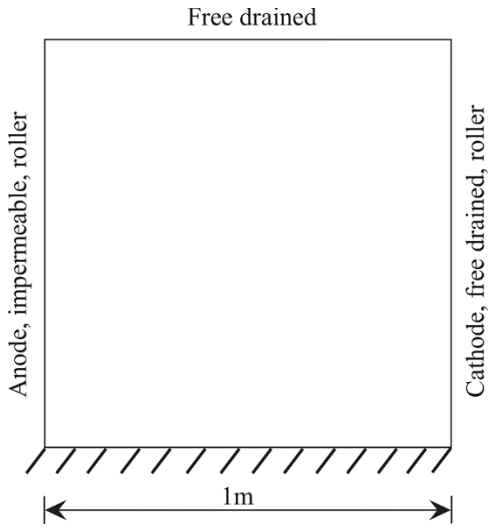

Figure 4. Applied input voltage in simulations for (**a**) intermittent current and (**b**) current reversal.

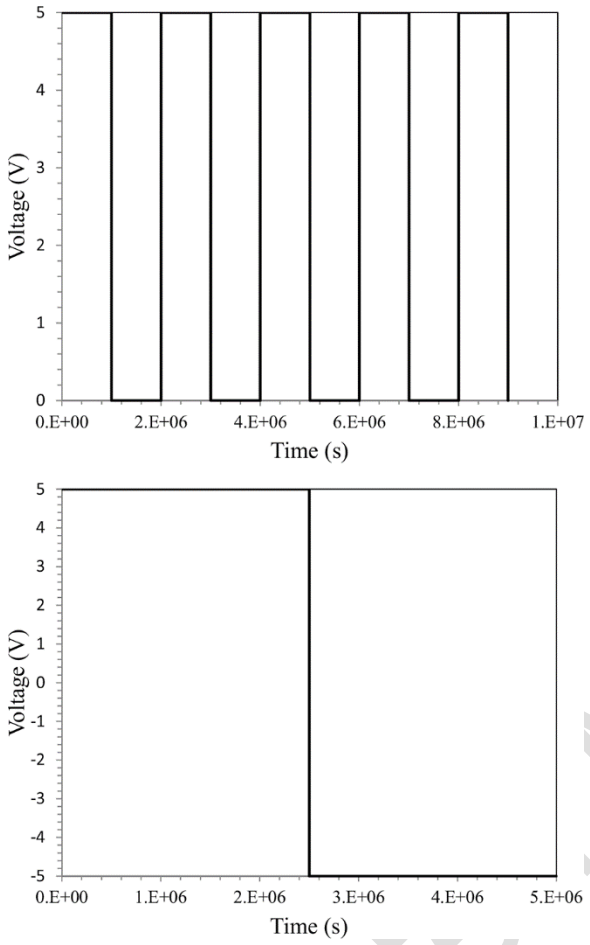

Figure 5. Influence of electrode configuration on evolution of (**a**) water outflow rate, (**b**) accumulated volume of water exiting, (**c**) electric current through the cathode and (**d**) energy consumption.

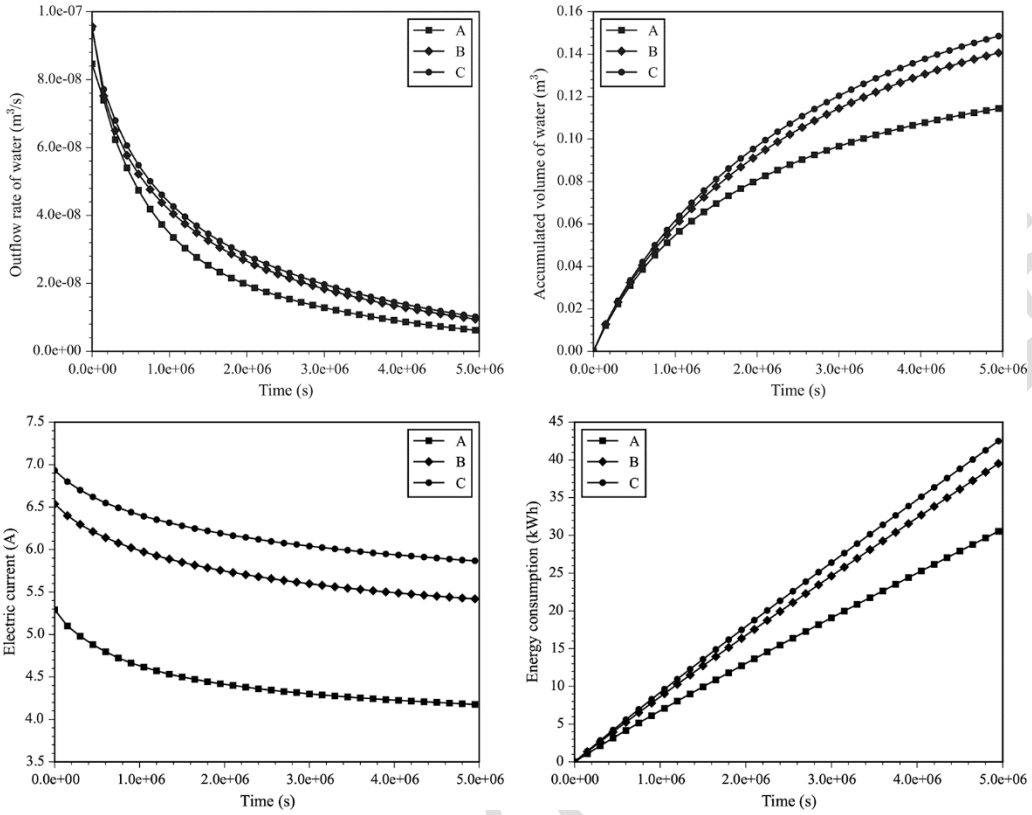

Figure 6. Influence of electrode configuration on (**a**) energy index, (**b**) KSI criterion and (**c**) coefficient of variation of settlement.

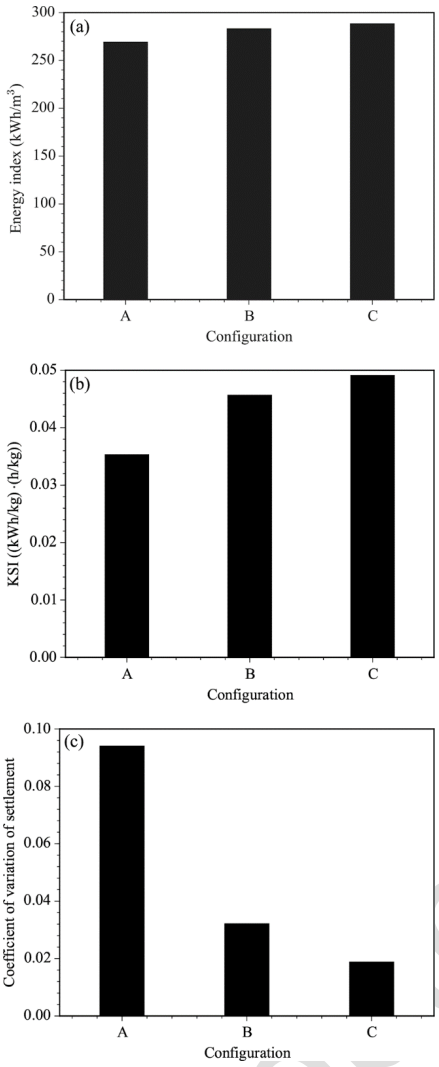

Figure 7. Influence of electrode spacing on evolution of (**a**) water outflow rate, (**b**) accumulated volume of water exiting, (**c**) electric current through the cathode and (**d**) energy consumption.

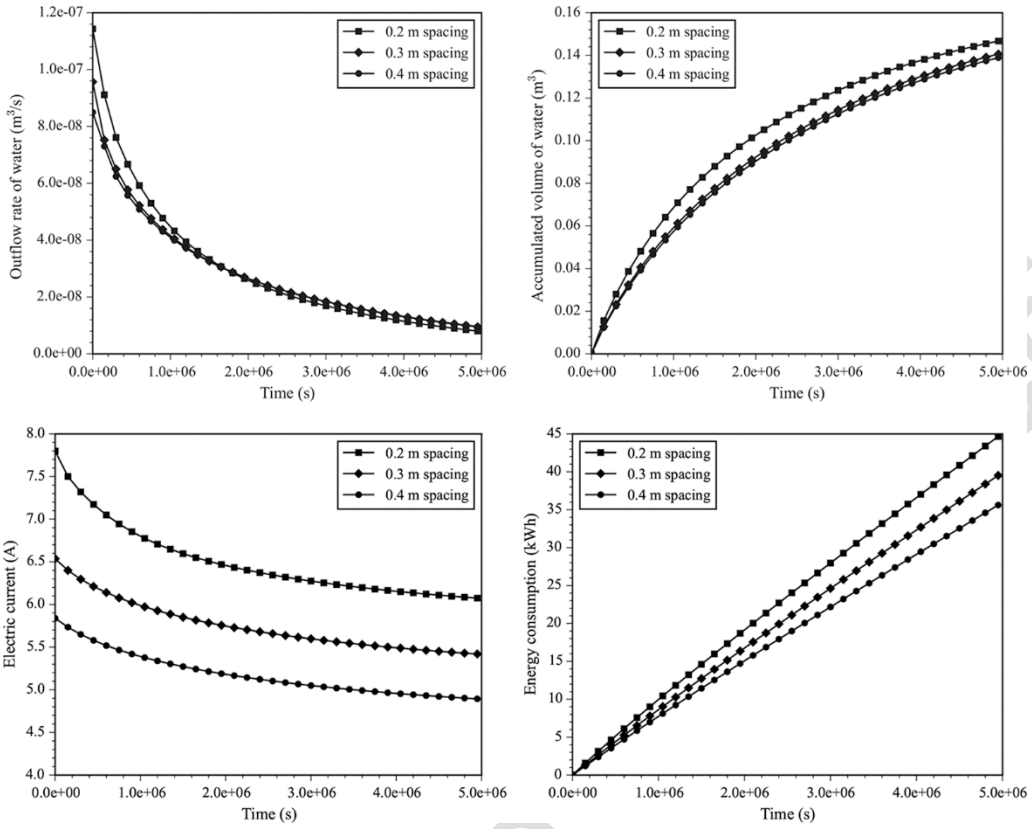

Figure 8. Influence of electrode spacing on (**a**) energy index and (**b**) KSI criterion.

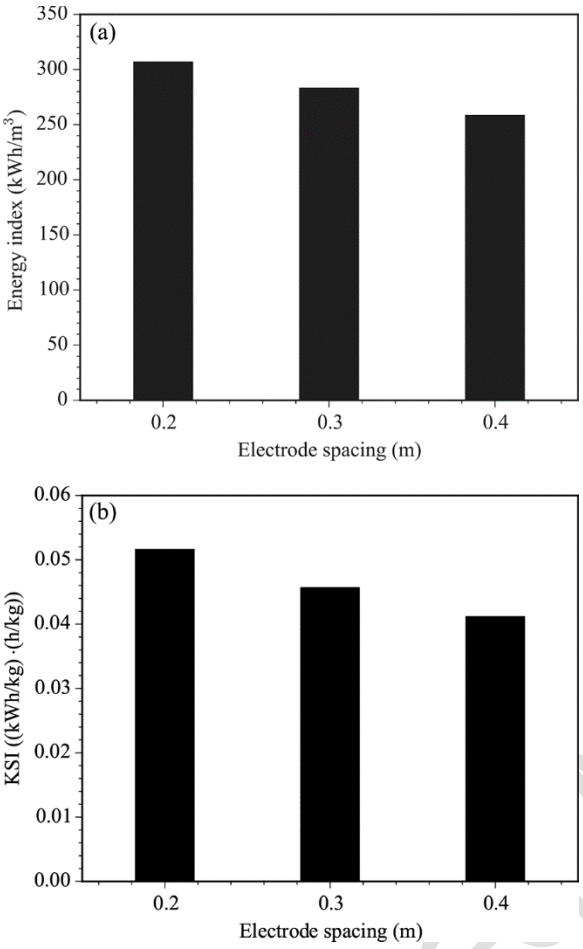

Figure 9. Influence of voltage gradient on evolution of (**a**) water outflow rate, (**b**) accumulated volume of water exiting, (**c**) electric current through the cathode and (**d**) energy consumption.

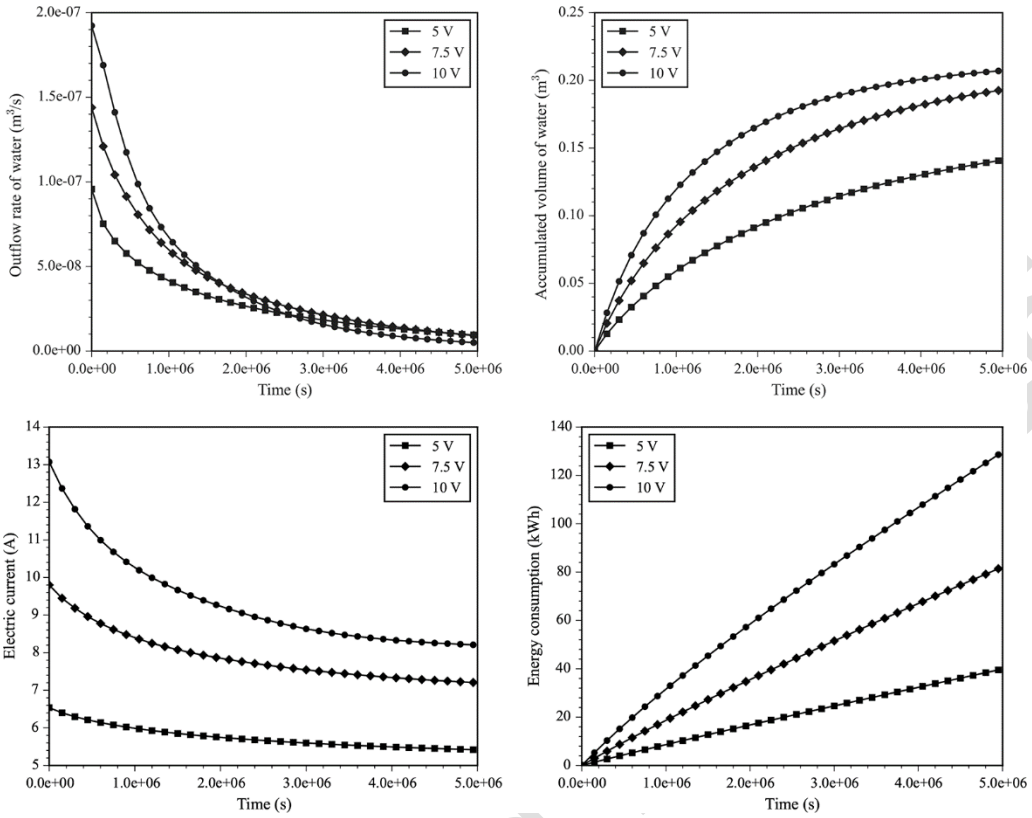

Figure 10. Influence of voltage gradient on (**a**) energy index and (**b**) KSI criterion.

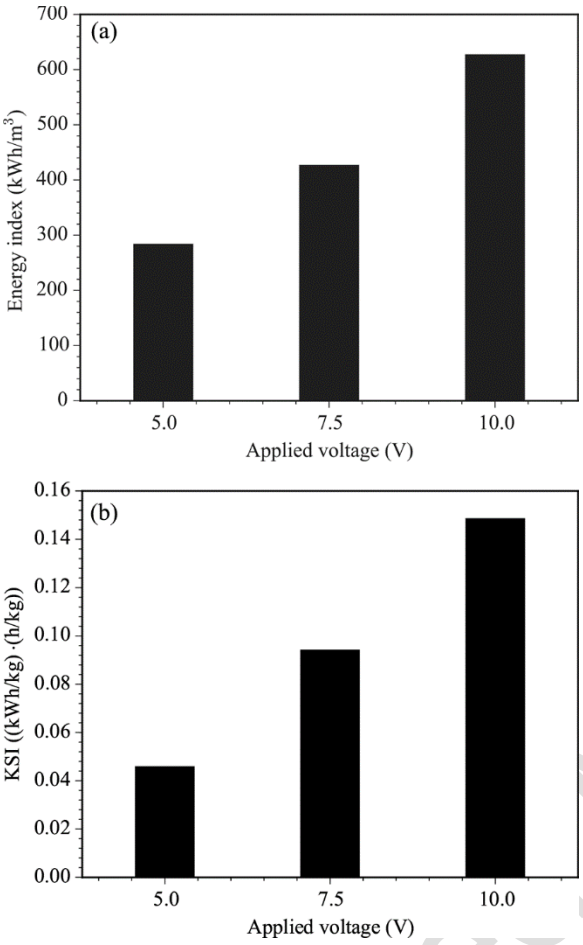

Figure 11. Influence of current intermittence on evolution of (**a**) pore water pressure at the bottom of the anode, (**b**) surface settlement at the top of the anode, (**c**) water outflow rate, (**d**) accumulated volume of water exiting, (**e**) electric current through the cathode and (**f**) energy consumption.

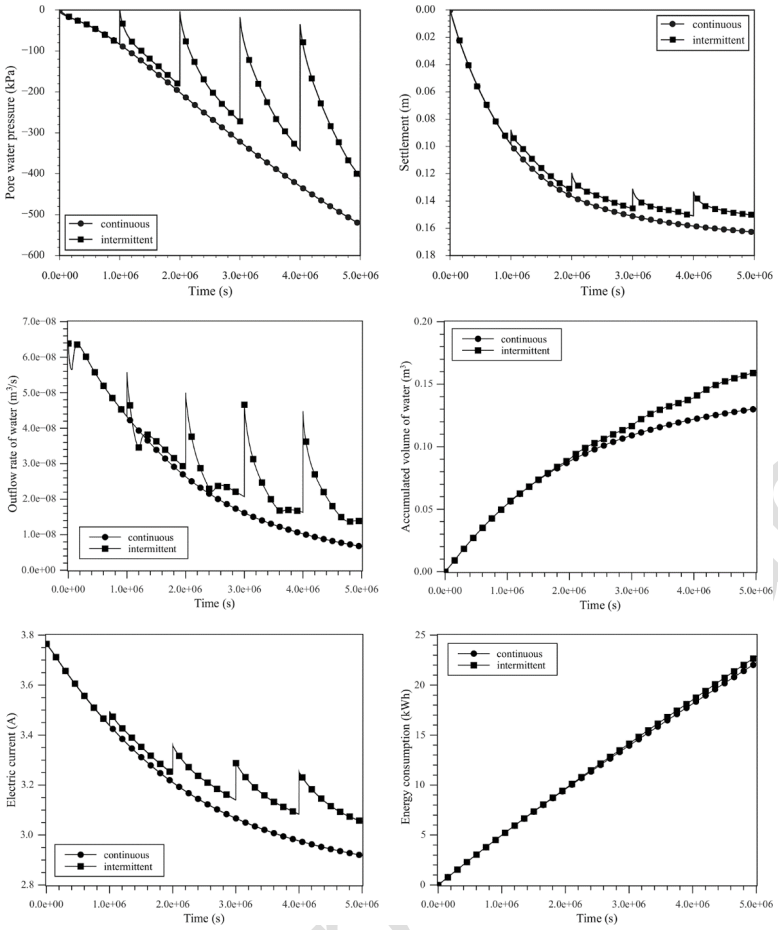

Figure 12. Comparison of (a) energy index and (b) KSI criterion for continuous and intermittent currents.

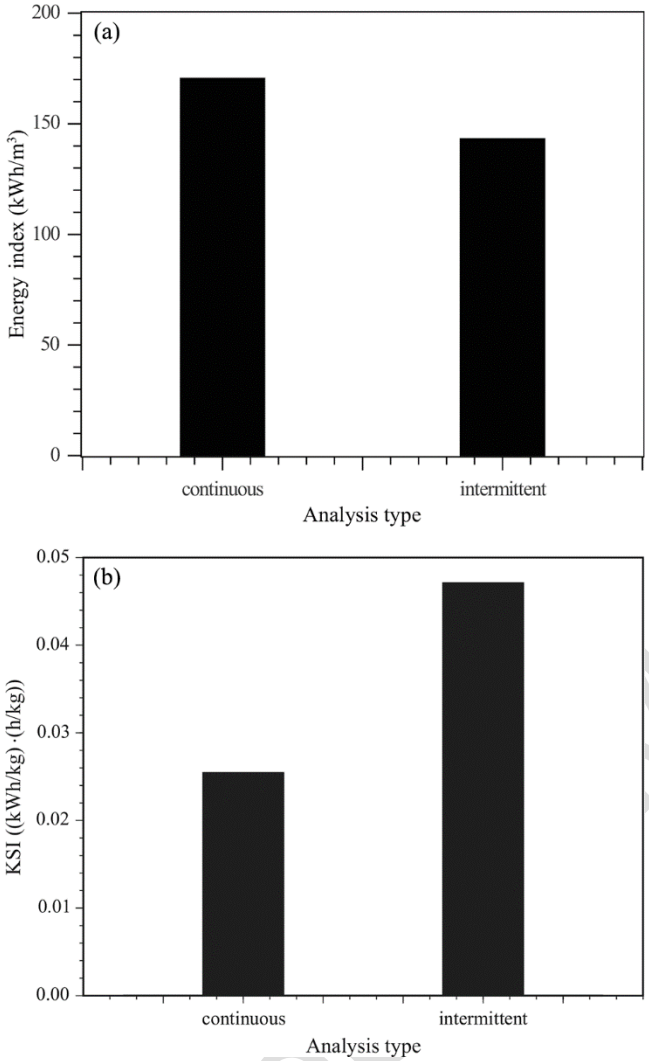

Figure 13. Influence of current intermittence on pore water pressure distributions: (**a**) after first intermittence (t 2.0 E + 06 seconds, see **Figure 4a**), (**b**) after second intermittence (at 4.0 E + 06 seconds), (**c**) after third intermittence (at 6.0 E + 06 seconds), (**d**) after fourth intermittence (at 8.0 E + 06 seconds), (**e**) final state (intermittent analysis) and (**f**) final state (continuous analysis)

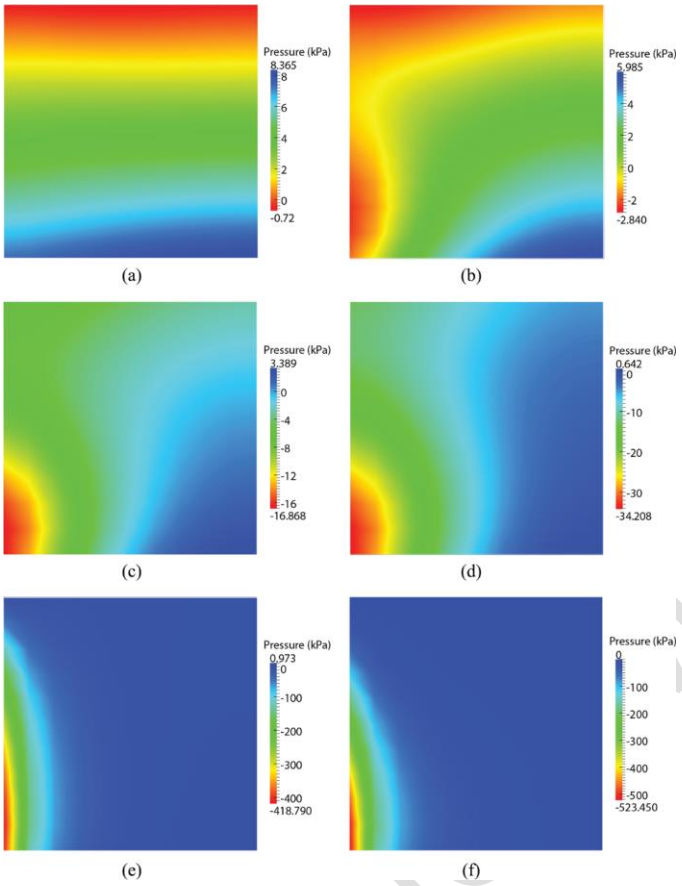

Figure 14. Influence of current reversal on evolution of (**a**) surface settlements at original anode and cathode, (**b**) water outflow rate through the cathode, (**c**) accumulated volume of water exiting through the cathode, (**d**) electric current through the cathode and (**e**) energy consumption.

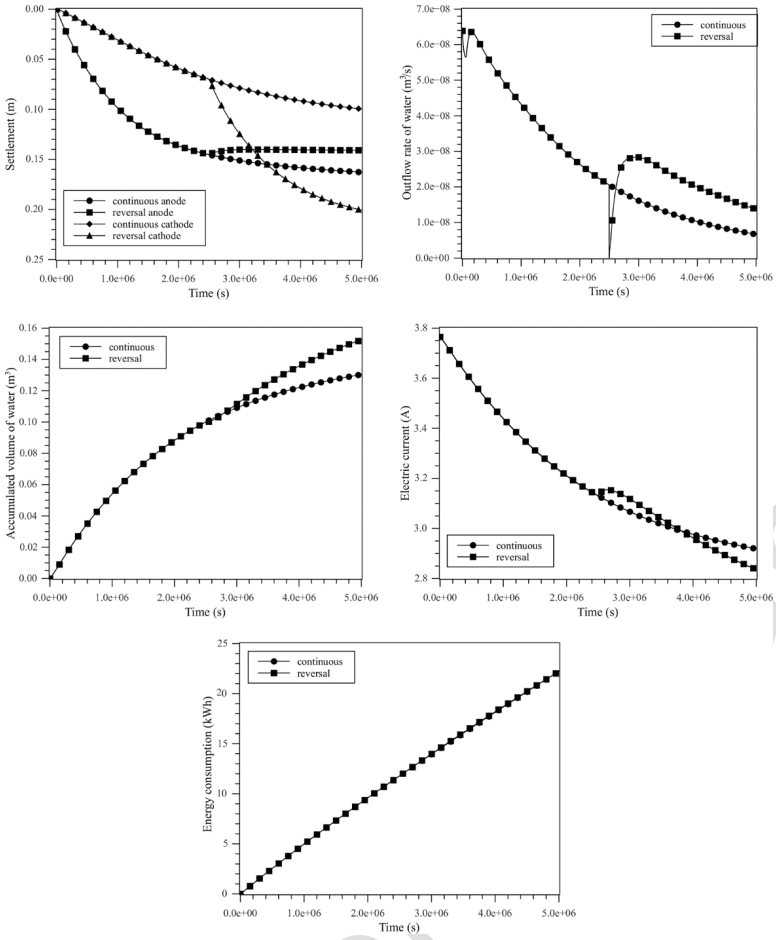

Figure 15. Comparison of (a) energy index and (b) KSI criteria for continuous and reversal currents.